scientific reports

Check for updates

OPEN

Blockade of persistent colored isomer formation in photochromic 3*H*-naphthopyrans by excited-state intramolecular proton transfer

Błażej Gierczyk[1], S. Shaun Murphree[2], Michał F. Rode[3]✉ & Gotard Burdzinski[4]✉

In photochemistry the excited-state intramolecular proton transfer process (ESIPT) is often observed as a highly efficient singlet excited state depletion pathway, which in the presence of a strong intramolecular hydrogen bond may proceed on a subpicosecond time scale. The present work describes the suppression of unwanted *transoid-trans* isomer formation in photochromic 3*H*-naphthopyran derivatives by the introduction of a 5-hydroxy substituent. According to time-resolved spectroscopy experiments and excited-state ab initio calculations, *transoid-cis* → *transoid-trans* photoisomerization is reduced by a competitive ESIPT channel in nonpolar solvent (cyclohexane). Upon specific solute–solvent interactions (methanol, acetonitrile) the intramolecular hydrogen bond in the *transoid-cis* form is perturbed, favoring the internal conversion $S_1 \rightarrow S_0$ process as photostabilizing channel.

The proton transfer (PT) reaction is known to play an important role in a variety of biological and physical processes[1]. A proton may be transferred in either the ground or the excited electronic state along the intramolecular hydrogen bond of the molecule, or along the intermolecular hydrogen bond in its complexes[2,3]. PT plays many important functions in nature, e.g. the excited-state intramolecular proton transfer (ESIPT) process is known to be responsible for photostability of DNA bases due to the presence of multiple intermolecular hydrogen bonds linking the base pairs[4–6]. Moreover, the ESIPT process is a common reaction in many internally H-bonded organic molecules[7–10] and thus may play an essential role in many applications, e.g., in organic photostabilizers[11–13]—the compounds used for protection of synthetic polymers against degradation caused by UV components of sunlight[14,15]. ESIPT can also lead to photochromic functionality, e.g. in Schiff bases[16]. The ESIPT phenomenon was utilized as a photoswitching mechanism in internally hydrogen-bonded molecules[17–19]. The search for proton cranes, in which a proton can be transferred over long distances through large-amplitude motion, is still a hot topic[20–22].

The ESIPT process specifically between a hydroxyl group and an adjacent carbonyl group has been observed to proceed with a small energy barrier in quite a few chemical families. For example, rapid ESIPT has been implicated as a key factor in the photostability of naturally occurring hydroxyanthraquinone red colorants found in art masterpieces and illuminated manuscripts[23]. Ab initio studies on 5,6-dihydroxyindole (in which the 5-hydroxyl tautomerizes to a carbonyl) suggest a barrierless ESIPT as the key energy shunt pathway responsible for the photoprotective properties of eumelanin[24]. A similar process occurs in hydroxychromones[25,26], hydroxyflavones[27], and hydroxyquinolones[28]. Furthermore, ESIPT can either be coupled to, or compete with other processes. For example, 3-hydroxypicolinic acid engages in a double ESIPT[19,29], and a designed quinoxalinylsalicylaldehyde can undergo either a normal ESIPT to the adjacent carbonyl, or an excited state long-range proton transfer (ESLRPT) to the more distant quinolinyl nitrogen, depending upon the excitation wavelength[30].

Importantly, the photophysics and photochemistry of molecular systems (especially their S_1-state energetic landscape) can be tuned by chemical modifications that may activate the ESIPT pathway[18,29,31], which upon strong intramolecular hydrogen bonding may proceed on subpicosecond time scale[32,33] and with high efficiency at the expense of other competitive reaction channels in the excited state. For instance, such a strategy can be used to

[1]Faculty of Chemistry, Adam Mickiewicz University in Poznań, Uniwersytetu Poznańskiego 8, 61-614 Poznań, Poland. [2]Department of Chemistry, Allegheny College, 520 North Main Street, Meadville, PA, USA. [3]Institute of Physics, Polish Academy of Sciences, Aleja Lotników 32/46, 02-668 Warsaw, Poland. [4]Faculty of Physics, Adam Mickiewicz University in Poznań, Uniwersytetu Poznańskiego 2, 61-614 Poznań, Poland. ✉email: mrode@ifpan.edu.pl; gotardb@amu.edu.pl

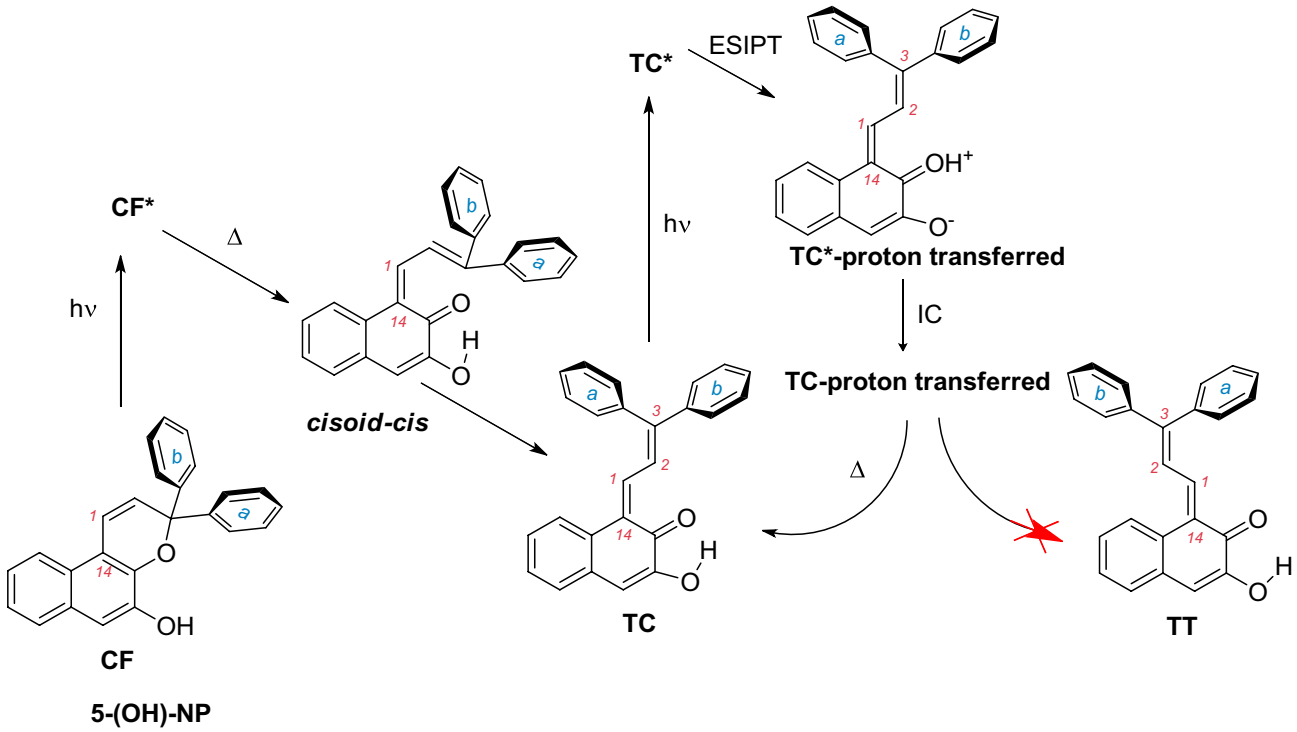

Figure 1. Expected photostabilization of the **TC** form due to the ESIPT process.

reduce triplet excited state formation in order to minimize side-effects in UV sunscreens (2-hydroxybenzophenone-based derivatives)[34]. Similarly, the present work leverages ESIPT to suppress the unwanted photochemical channel of *transoid-cis* → *transoid-trans* photoisomerization in 3*H*-naphthopyrans (**NP**). For this purpose, we chose 5-hydroxy-**NP** (**5-(OH)-NP**) as a model compound (Fig. 1).

3H-Naphthopyrans constitute a unique family of compounds that not only have advantageous photochromic properties for use in commercially available photochromic lenses, but also can be easily synthetically modified to obtain desired spectroscopic and photophysical properties[35–38]. The UV-induced coloration in **NP** compounds occurs via a barrierless photodissociative ring opening of the colorless pyranoid closed form (**CF**), leading to the formation of a colored open-form *transoid-cis* (**TC**) isomer[39]. During this process, or upon **TC** photoexcitation, a *transoid-trans* (**TT**) side product is produced if the excited-state energy landscape favours a *single-twist* rotation along the C_{14}=C_1 axis[40,41]. However, the presence of **TT** in photochromic systems may be unwanted in some applications, such as photochromic lenses, due to the substantially longer **TT** vs. **TC** lifetime (hours vs seconds), which leads to prolonged fading rates after the cessation of UV exposure[40,42]. The thermal fading **TT** → **TC** is hampered by a high energy barrier (ca. 1.3 eV[39]).

In this study we demonstrate with the 5-hydroxy-**NP** model compound that **TT** formation can be suppressed by the intervention of ESIPT. This principle may be important for the development of ESIPT-based **NP** derivatives for photochromic materials with reduced **TT** contribution.

Experimental

Materials. 3,3-Diphenyl-5-hydroxy-3*H*-benzo[*f*]chromene (**5-(OH)-NP**) was synthesized following the procedures described in the Supplementary Information. In the time-resolved spectroscopic investigations cyclohexane, methanol and acetonitrile of spectroscopic grade from Sigma Aldrich were used for solution preparation. Studies were performed vs. a reference compound 3,3-diphenyl-3*H*-naphtho[2,1-*b*]pyran (**5-(H)-NP**) purchased from TCI.

Time-resolved UV–Vis spectroscopy. Changes in UV–Vis absorption spectra and kinetics on a time scale of seconds were recorded for solutions in a 1 cm × 1 cm fused silica cuvette. Conditions of 21 °C were achieved by placing the sample into a temperature-controlled cuvette holder (Flash 300, Quantum Northwest) with stirring switched on. UV LED (λ_{exc} = 340 nm, Thorlabs M340L4) was used to induce the photochromic reaction. UV–Vis probing light was generated by a xenon lamp (Applied Photophysics), equipped with a bundle fiber. The probing beam was passed through a long-pass filter (WG 280) and an almost-closed iris to ensure low light intensity in the cell. The UV–Vis spectra were recorded by an Ocean Optics FLAME-T-VIS-NIR-ES USB spectrometer at the sampling rate of 20 spectra per second.

Femtosecond UV–Vis transient absorption spectra were obtained using a commercially available system (Ultrafast Systems, Helios)[43]. The ultrafast laser system consists of a short-pulse titanium-sapphire oscillator (Mai-Tai, Spectra Physics, 70 fs) followed by a high-energy titanium-sapphire regenerative amplifier (Spitfire Ace, Spectra Physics, 100 fs). The 800 nm beam was split into two beams to generate: (1) a pump (λ_{exc} = 444 nm)

in the optical parametric amplifier (Topas Prime with a NirUVis frequency mixer) and (2) probe pulses—white light continuum in the UV–Vis (330–660 nm) range by using CaF_2 plate. The remaining 800 nm photons in the probe pulse were filtered out before the sample: **5-(OH)-NP** solution in a quartz cell 2 mm thick with stirring. Photostationary state of **TC** population was obtained by the continuous UV LED irradiation at 340 nm. For selective excitation of the **TC** population, the excitation wavelength was set at $\lambda_{exc} = 444$ nm with a pump pulse energy of 1 μJ. The transient absorption data were corrected for chirp of white light continuum.

The obtained transient absorption spectra were analyzed using the global fitting procedure (ASUFIT program) and satisfactory fits were obtained with single- or double-exponential fits. Convolution with the instrument response function (200 fs, FWHM) was included in the fitting procedure. The accuracies of the obtained time-constants derived from analysis of transient absorption results were as follows: 5% (UV–Vis data in time window over tens/hundreds of seconds) and 10% (ultrafast UV–Vis data).

Computational details. The equilibrium geometries of the **5-(OH)-NP** isomers in their closed-shell ground state (S_0) were obtained with the MP2 method[44] without imposing any symmetry constraints. The energy of the most stable form $\mathbf{CF_1}$ is the reference energy for higher energy structures. The excited-state (S_1) equilibrium geometries were determined with the second-order algebraic diagrammatic construction ADC(2) method[45–47]. The correlation-consistent valence double zeta basis set with polarization functions on all atoms (cc-pVDZ)[48] was used in these calculations, as well as in potential energy profiles and surfaces. The vertical excitation energies and response properties of the lowest excited singlet states were calculated using the CC2 methods[49,50]. The basis set augmented with the diffuse functions aug-cc-pVDZ was also used to compute vertical excitation energies of the molecular system. All calculations were performed using the TURBOMOLE program package[51].

Results and discussion

Ground state energy landscape and vertical excitation energies of 5-(OH)-NP. The studied 5-hydroxy 3*H*-naphthopyran (**5-(OH)-NP**) possesses two closed-pyran **CF** minima in the ground electronic state (S_0). The most stable is the $\mathbf{CF_1}$ form, which is stabilized by the O_5–H· · ·O_4 hydrogen-bond between the two neighboring oxygen atoms (Table 1). The second $\mathbf{CF_2}$ minimum, with the hydroxyl group rotated about 180°, is 0.156 eV higher in energy. As shown in Table 1, the $S_0 \rightarrow S_2$ absorption maximum (strongest absorption) of the H-bonded $\mathbf{CF_1}$ form is bathochromic by 0.12 eV vs. the rotated $\mathbf{CF_2}$ form. Photoexcitation of the colorless **CF** form ($\mathbf{CF_1}$ or $\mathbf{CF_2}$) leads to the respective colored isomers ($\mathbf{TC_1}$ or $\mathbf{TC_2}$, respectively) in a barrierless process in the S_1 excited state, the behaviour of which is similar to the previously studied unsubstituted parent **NP** molecule[39]. The photogenerated $\mathbf{TC_1}$ conformer is also stabilized by an intramolecular hydrogen bond *vs.* the rotated $\mathbf{TC_2}$ compartment, (0.407 eV vs. 0.752 eV). Such a large stabilization energy causes the $\mathbf{TC_1}$ form to predominate over the $\mathbf{TC_2}$ population under typical experimental conditions.

The calculated S_0-state energy barrier for free rotation of the hydroxyl group ($\mathbf{TC_2} \rightarrow \mathbf{TC_1}$) is + 0.17 eV or + 0.18 eV, depending on the rotation side (MP2/cc-pVDZ). Again, similar to **CF**, the absorption maximum of H-bonded $\mathbf{TC_1}$ is slightly red-shifted *vs.* the rotated $\mathbf{TC_2}$ isomer (see Table 1). Stabilization of $\mathbf{TC_1}$ by intramolecular hydrogen bonding explains why for freshly prepared solutions of **5-(OH)-NP** a small amount of **TC** species is observed by a weak absorption band with maximum at 443 nm (Fig. S1). Its content is roughly estimated at 0.8% in cyclohexane, and a similar amount of 1.0–1.5% was estimated in $CDCl_3$ by ^{1}H-NMR spectra integration (see Supplementary Information). Interestingly, the **TC** band absorption is less pronounced in methanol and acetonitrile (Fig. S1), likely due to disruption of the internal hydrogen bond in **TC** by solute–solvent specific interactions. Such an equilibrium between **TC** and **CF** has been reported for a similar **NP** derivative[52]. To explore this phenomenon, various **TC** and methanol (1:1) complexes were calculated (Fig. S2A). The most stable complex is **MC1** with one hydrogen bond formed between the O_5H hydroxyl group and the methanol acting as a proton acceptor, and a second H-bond formed between the O_4 oxygen atom and the methanol acting as a proton donor. Such double hydrogen bond formation stabilizes the **TC–methanol** complex. However, the intramolecular hydrogen bond is weakened (length is 2.373 Å, Fig. S2A) vs the isolated **TC** molecule in the gas phase (1.947 Å). In the case of complexes with acetonitrile (Fig. S2B), interactions are related to ππ stacking interactions and hydrogen bonding.

Thermally activated fading process of the TC isomer to colorless CF. The **TC** isomer plays a key role as a coloured species in the photochromic reaction of **NP** derivatives. **TC** decay occurs in a two-step reaction leading to **CF** via a high-in-energy *cisoid-cis* intermediate **INT** form. The timescale of the **TC** form depopulation depends strongly on the ratio of the S_0 state energy barriers, ΔE, separating this *cisoid-cis* intermediate from the neighboring stable conformers: colored **TC** ($\Delta E^{INT\text{-}TC}$) and colorless **CF** ($\Delta E^{INT\text{-}CF}$), see Fig. 2[41,53].

The $\mathbf{TC_1}$ relative energy of 0.407 eV for **5-(OH)-NP** is much lower than that for the **5-(H)-NP** derivative (0.588 eV)[39], mainly due to the internal hydrogen bond in the $\mathbf{TC_1}$ form of **5-(OH)-NP**. Conversely, the larger relative energy of $\mathbf{TC_2}$ (0.752 eV) is due to O_4· · ·O_5 repulsion, which is absent in **5-(H)-NP**. The relative energy of the rotated $\mathbf{TC_2}$ isomer is higher (0.752 eV) than that of $\mathbf{TC_1}$ (0.407 eV); consequently, in inert solution such as cyclohexane the equilibrium is shifted towards $\mathbf{TC_1}$.

The **TC** isomers constitute relatively deep minima on the S_0-state minimum potential-energy profile, separated from the **INT** intermediate by the $\Delta E^{TC\text{-}out}$ energy barrier of + 0.466 eV in the case of H-bonded $\mathbf{TC_1}$ (Table 2), which is slightly larger than for **5-(H)NP** (+ 0.452 eV)[39]. Despite the large barrier, the process leading to **CF** is thermally available due to its exothermic character. However, the high-in-energy intermediate **INT** must first be populated. Once **INT** is formed, it turns out that the energy barrier ($\Delta E^{INT\text{-}CF1}$) for the forward process ($\mathbf{INT_1} \rightarrow \mathbf{CF_1}$) is much larger (+ 0.313 eV) than the corresponding barrier ($\Delta E^{INT\text{-}TC1}$) toward $\mathbf{TC_1}$ (+ 0.235 eV).

S_0 form		ΔE^{VE}	λ_{abs}	f	μ_e
Colorless CF forms					
5-(OH)-CF (H-bonded), CF_1 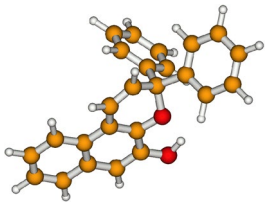	S_0	0.00			$\mu_g = 2.3$
	$S_0 \rightarrow S_1(\pi\pi^*)$	3.81		0.035	1.00
	$S_0 \rightarrow S_2(\pi\pi^*)$	3.88	**320**	**0.208**	2.74
	$S_0 \rightarrow S_3(n\pi^*)$	4.71		0.009	2.32
	$S_0 \rightarrow S_4(\pi\pi^*)$	4.75		0.058	3.35
	$S_0 \rightarrow S_5(n\pi^*)$	4.88		0.009	6.26
5-(OH)-CF (rotated), CF_2 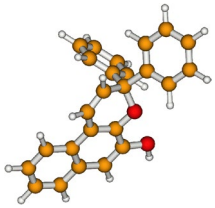	S_0	0.156[a]			$\mu_g = 1.1$
	$S_0 \rightarrow S_1(\pi\pi^*)$	3.81		0.036	1.55
	$S_0 \rightarrow S_2(\pi\pi^*)$	4.00	**310**	**0.176**	3.87
	$S_0 \rightarrow S_3(n\pi^*)$	4.69		0.000	3.44
	$S_0 \rightarrow S_4(n\pi^*)$	4.81		0.003	8.26
Colored TC forms					
5-(OH)-TC (H-bonded), TC_1 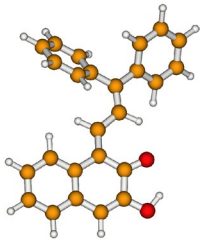	S_0	0.407[a]			$\mu_g = 3.8$
	$S_0 \rightarrow S_1(\pi\pi^*)$	2.55	486	0.075	6.75
	$S_0 \rightarrow S_2(\pi\pi^*)$	2.96	**420**	**0.771**	6.27
	$S_0 \rightarrow S_3(n\pi^*)$	3.14		0.016	0.79
	$S_0 \rightarrow S_4(\pi\pi^*)$	4.01		0.093	5.77
5-(OH)-TC (rotated), TC_2 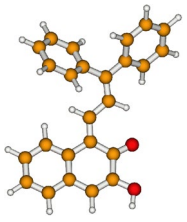	S_0	0.752[a]			$\mu_g = 2.5$
	$S_0 \rightarrow S_1(\pi\pi^*)$	2.73	453	0.175	4.15
	$S_0 \rightarrow S_2(\pi\pi^*)$	2.87	432	0.186	3.12
	$S_0 \rightarrow S_3(\pi\pi^*)$	3.13	**396**	**0.509**	4.63
	$S_0 \rightarrow S_4(\pi\pi^*)$	4.09		0.105	4.52
	$S_0 \rightarrow S_5(n\pi^*)$	4.32		0.004	9.09
	$S_0 \rightarrow S_6(\pi\pi^*)$	4.40		0.205	3.17
Colored TT forms					
Continued					

S_0 form		ΔE^{VE}	λ_{abs}	f	μ_e
5-(OH)-TT (H-bonded), TT_1 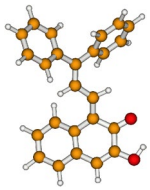		0.438[a]			$\mu_g = 3.7$
	$S_0 \rightarrow S_1(\pi\pi^*)$	2.68	463	0.122	5.82
	$S_0 \rightarrow S_2(\pi\pi^*)$	3.06	**405**	**0.670**	7.42
	$S_0 \rightarrow S_3(\pi\pi^*)$	3.33		0.023	1.08
	$S_0 \rightarrow S_4(\pi\pi^*)$	4.11		0.062	5.72
	$S_0 \rightarrow S_5(\pi\pi^*)$	4.37		0.216	2.89
	$S_0 \rightarrow S_6(\pi\pi^*)$	4.39		0.022	11.96
5-(OH)-TT (rotated), TT_2 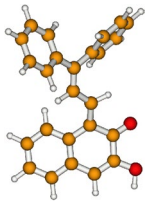		0.760[a]			$\mu_g = 2.8$
	$S_0 \rightarrow S_1(\pi\pi^*)$	2.82	**440**	**0.206**	3.92
	$S_0 \rightarrow S_2(\pi\pi^*)$	3.11	**399**	**0.308**	1.40
	$S_0 \rightarrow S_3(\pi\pi^*)$	3.25	**381**	**0.284**	5.48
	$S_0 \rightarrow S_4(\pi\pi^*)$	4.20		0.074	4.55
	$S_0 \rightarrow S_5(\pi\pi^*)$	4.37		0.178	4.88
	$S_0 \rightarrow S_6(\pi\pi^*)$	4.46		0.028	8.22

Table 1. Vertical excitation energy, ΔE^{VE} (in eV) and λ_{abs} (in nm), oscillator strength, f, and dipole moment, μ_e (in Debye), of the lowest excited singlet states calculated with the CC2/aug-cc-pVDZ method for the **5-(OH)-NP** ground state equilibrium forms optimized at the MP2/cc-pVDZ theory level. Dipole moment of the ground-state, μ_g (in Debye, MP2/cc-pVDZ). [a]Difference in adiabatic energy (E^a, in eV) relative to the closed form, $\mathbf{CF_1}$, calculated at the MP2/cc-pVDZ theory level. Significant values are in [bold].

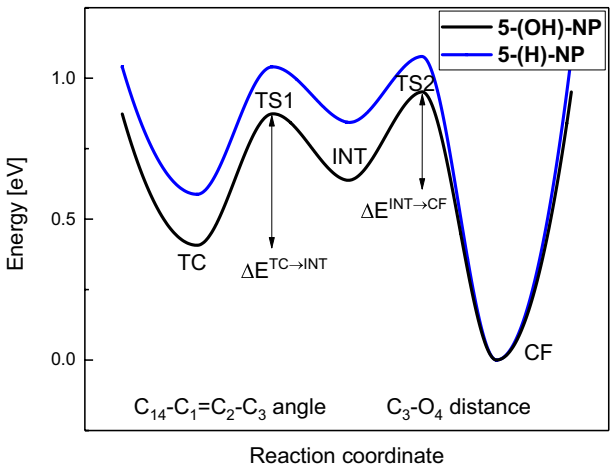

Figure 2. Thermal decoloration of **TC → CF** for **5-(OH)-NP** compound (black line) involves two reaction steps **TC → INT** and **INT → CF** (the first step is reversible). S_0-state potential-energy profiles were computed with aid of the MP2/cc-pVDZ method. The reference compound **5-(H)-NP** (blue curve) is traced according to reported data[53].

Thus, one can expect recovery of the $\mathbf{TC_1}$ isomer as the most probable path (Fig. 2), which suggests a rationale for the long apparent $\mathbf{TC_1}$ lifetime in solution for **5-(OH)-NP** vs. **5-(H)-NP**.

Apparent TC fading rate and lack of TT population in changes of UV–Vis absorption spectra. In our previous studies of **NP** photochromic reactions, LED light at λ = 365 nm was used for

Form	TC E^a/eV μ_g/D	$\Delta E^{TC\text{-}out}$	TS2 E^a/eV μ_g/D	$\Delta E^{INT\text{-}TC}$	INT E^a/eV μ_g/D	$\Delta E^{INT\text{-}CF}$	TS1 E^a/eV μ_g/D	CF E^a/eV μ_g/D
	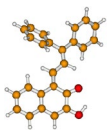		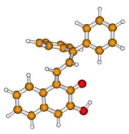		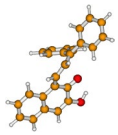		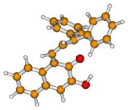	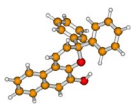
5-(OH)-NP (H-bonded)	0.407 3.8	+0.466	0.873 2.0	+0.235	0.638 2.3	+0.313	0.951 2.9	0.00 2.60
	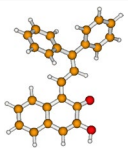		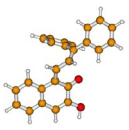		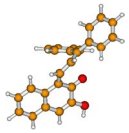		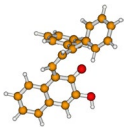	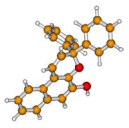
5-(OH)-NP (rotated)	0.752 2.5	+0.431	1.183 2.7	+0.197	0.986 1.5	+0.246	1.232 0.3	0.156 1.1
	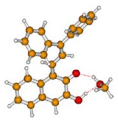		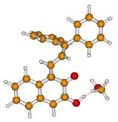		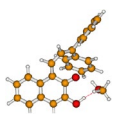		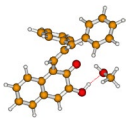	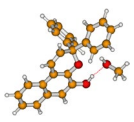
5-(OH)-NP with methanol **MC1**	0.555 4.9	+0.437	0.992 2.6	+0.252	0.740 3.0	+0.281	1.021 3.7	0.000 3.8
	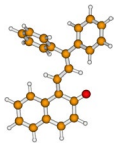		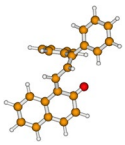		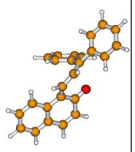		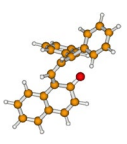	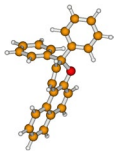
5-(H)-NP	0.588 2.8	+0.452	1.040 2.9	+0.196	0.844 1.5	+0.233	1.077 0.7	0.000 0.9

Table 2. Energetics of the two-step process of the **TC** form depopulation (**TC** ↔ **INT** → **CF**) for **5-(OH)-NP** vs. **5-(H)-NP**. Adiabatic S_0-state energies, E^a, in eV, and dipole moment, μ_g, in Debye, for the relevant minima: **TC**, **INT**, **CF**, and transition states separating these minima: **TS1** and **TS2**, calculated at the MP2/cc-pVDZ theory level. Results for **5-(H)-NP** are from reference[53].

photoexcitation[39–41]. However, since the **5-(OH)-NP** absorption spectrum is blue-shifted in comparison to **5-(H)-NP** (see Fig. S1), LED light at λ = 340 nm was selected for this investigation. UV irradiation of **5-(OH)-NP** in cyclohexane for 60 s produces a photostationary state (PSS, Fig. 3A).

Figure 3B shows that the initial rise of the **TC** absorption signal is very similar to **5-(H)-NP**, so one can estimate a similar quantum yield for **TC** formation in cyclohexane (0.745[39]). Figure 3C presents the evolution of absorption for **5-(OH)-NP** after ceasing UV irradiation at the moment t = 0 s. The initial absorption spectrum shows a positive **TC** absorption band with a maximum at 443 nm, and a negative band at 343 nm due to **CF** bleach. Subsequently, the decay of the **TC** band occurs more slowly in **5-(OH)-NP** than for **5-(H)-NP** (Fig. 3C *vs.* 3D), with apparent **TC** lifetimes at 21 °C of 66 s and 9.2 s, respectively, according to global analysis (see Fig. S3).

Note that this **TC** lifetime elongation effect was predicted by theoretical calculations (section above). Upon decay of the **TC** absorption band, a practically baseline level is reached after a few hundreds of seconds (Fig. 3C), in contrast to **5-(H)-NP** (Fig. 3D), which shows the presence of the **TT** absorption band. This demonstrates that insertion of the hydroxyl group at position 5 suppresses the **TT** formation channel. A substantial **TT** reduction is clearly observed (compare Fig. 3C *vs.* 3D), and only a very low concentration of **TT** can be detected for **5-(OH)-NP** (see Fig. S3). The reduced yield of the photoisomerization path **TC** → **TT** could be explained by a strong competitive channel, which is probably ESIPT in cyclohexane. As we mentioned above, the intramolecular hydrogen bond in **TC** (from **5-(OH)-NP**) is likely disrupted in methanol or acetonitrile solution, so the ESIPT process is less probable in these solvents. Nevertheless, reduced **TT** formation is observed (see Figs. S4 and S5). The photostabilization of the **TC** species in these solvents is probably mediated by solvent polarity[54]—note that calculated dipole moment for **TC** in the S_1 state is high (Table 1). Stabilization of **TC** in the S_1 state in polar solvent may facilitate conical intersection CI (S_1/S_0) leading to the S_0 state with a less advanced change in the twist angle C_{14}=C_1, thus **TT** formation is disfavored. This trend, although less pronounced, has been already observed for the parent compound **5-(H)-NP** in acetonitrile[54].

According to Table 3, the apparent S_0 ground state **TC** lifetime is longer for **5-(OH)-NP** vs. **5-(H)-NP**. The largest difference is observed in cyclohexane (factor of 7) due to the presence of the intramolecular hydrogen bond for **5-(OH)-NP** stabilizing the **TC** form. The presumed breaking of the intramolecular H-bond in

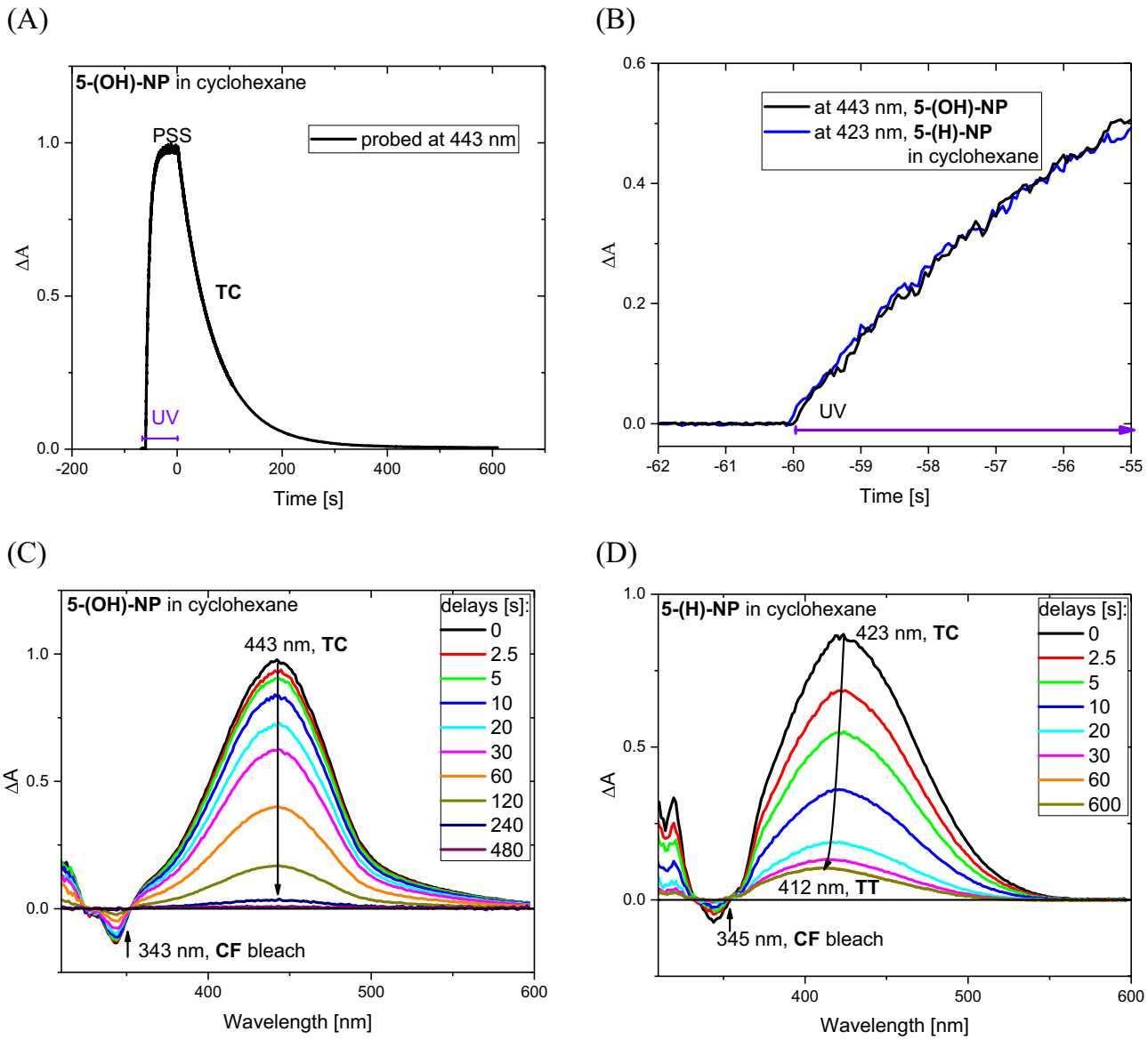

Figure 3. (**A**) Changes in absorption at probe 443 nm caused by UV irradiation. (λ = 340 nm, 4 mW/cm^2) of **5-(OH)-NP** in cyclohexane at 21 °C. (**B**) The initial rise in absorption upon switching on UV irradiation for two solutions **5-(OH)-NP** and **5-(H)-NP** in cyclohexane prepared with the same absorption (A(340 nm, 1 cm) = 0.32). (**C**, **D**) Evolution of ΔA spectra after ceasing UV irradiation at t = 0 s for **5-(OH)-NP** and **5-(H)-NP**, respectively.

Compound	Solvent	S_0(TC) λ_{abs}^{max}, nm	τ_{S0}, s
5-(OH)-NP	Cyclohexane	443	66
	Acetonitrile	443	27.5
	Methanol	437	50
5-(H)-NP	Cyclohexane	423	9.2
	Acetonitrile	427	8.5
	Methanol	434	12

Table 3. Photophysical properties of **TC** in solution: S_0 absorption band maximum and lifetime τ_{S0} with 5% accuracy (at 21 °C).

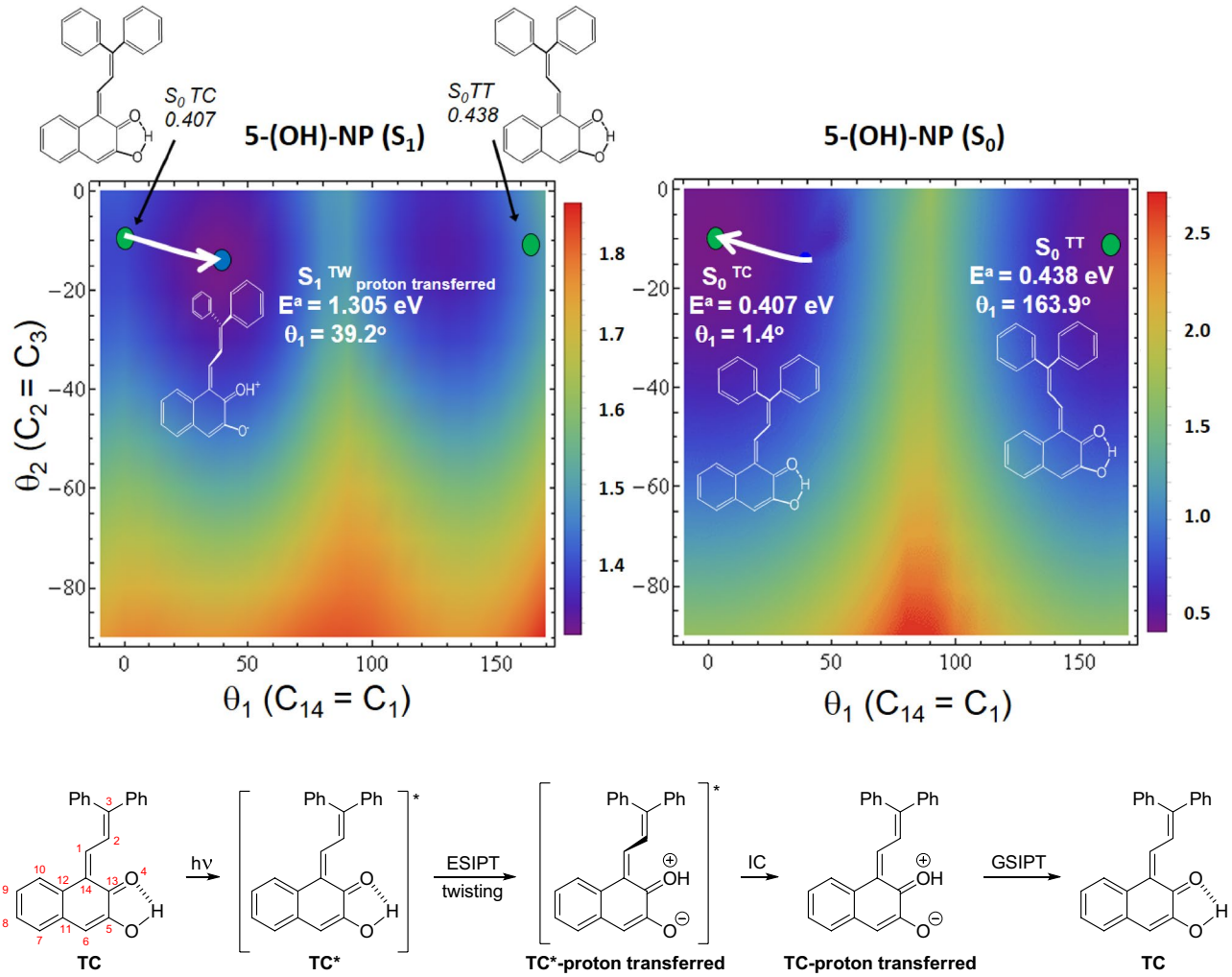

Figure 4. Minimum potential-energy surface of the lowest excited (left) and the ground electronic state (right) of the **5-(OH)-TC** (H-bonded) species mimicking system evolution, plotted as a function of $\theta_1(C_{14}{=}C_1)$ and $\theta_2(C_2{=}C_3)$ torsional angle coordinates. Green circles represent the Franck–Condon regions of the ground-state $\mathbf{S_0}^{\mathbf{TC}}$ and $\mathbf{S_0}^{\mathbf{TT}}$ local minima. Blue circle represents $\mathbf{S_1}^{\mathbf{TC}}$ minimum populated after $\mathbf{S_0}^{\mathbf{TC}}$ photoexcitation. White arrows show the evolution of the system. The results were obtained with the aid of the ADC(2)/cc-pVDZ method, for the excited state (S_1), and with the MP2/cc-pVDZ, for the ground state (S_0). The reaction scheme below shows steps in the photocycle free from **TT** generation.

polar solvents such as methanol and acetonitrile has been also postulated for structurally related 3-hydroxychromone[26,55]. Even if a weakened intramolecular hydrogen bond in **TC** is present in methanol (Fig. S2), calculations performed for **MC1** complex show a decrease in the $\Delta E^{INT\text{-}CF}$ barrier and an increase in $\Delta E^{INT\text{-}TC}$ barrier in comparison to the isolated **5-(OH)-NP** (H-bonded) molecule (see Table 2). Thus, the shortening of the S_0 **TC** lifetime in methanol in relation to cyclohexane can be rationalized.

Properties of the excited TC isomer. For most **NP** derivatives photoexcitation of the **TC** isomer to its Franck–Condon region results in an excited S_1-state geometrical relaxation, in which rotations about the two double bonds $C_{14}{=}C_1$ and $C_2{=}C_3$ are activated[40,41]. But in **5-(OH)-TC** the S_1 state relaxation is additionally accompanied by the barrierless excited-state intramolecular proton transfer (ESIPT) from O_5 to O_4 to produce a proton-transferred species. The minimum energy of the **TC***-proton transferred species of **5-(OH)-NP** was found to be lower in energy ($E^a = 1.305$ eV) *vs*. the corresponding **TC*** species from **5-(H)-NP** ($E^a = 1.948$ eV)[40], due to presence of the stabilizing intramolecular hydrogen bond $O_5 \cdots H\text{-}O_4$ (see Fig. 4). Another observation is that the relaxed S_1 **TC** minimum occurs with an optimized θ_1 ($C_{14}{=}C_1$) dihedral angle of ~ 39° (see left square in Fig. 4), much lower than 90°, where the S_0-state energy barrier is seen (right square in Fig. 4). Thus, upon $S_1 \rightarrow S_0$ internal conversion, a species in the S_0 state is produced with geometry which, in the next step, follows the S_0-state gradient toward the S_0 **TC** global minimum. This barrierless process confirmed by geometry optimization is accompanied by the back proton transfer from O_4 to the O_5 oxygen atom (i.e. ground state intramolecular proton transfer, GSIPT). Note that alternative pathways, such as **TC** → **TT** isomerization, are suppressed due to a S_0-state high-energy wall (Fig. 4). Moreover, note that the $\theta_1(C_{14}{=}C_1)$ dihedral angle of 39° found for the **TC**

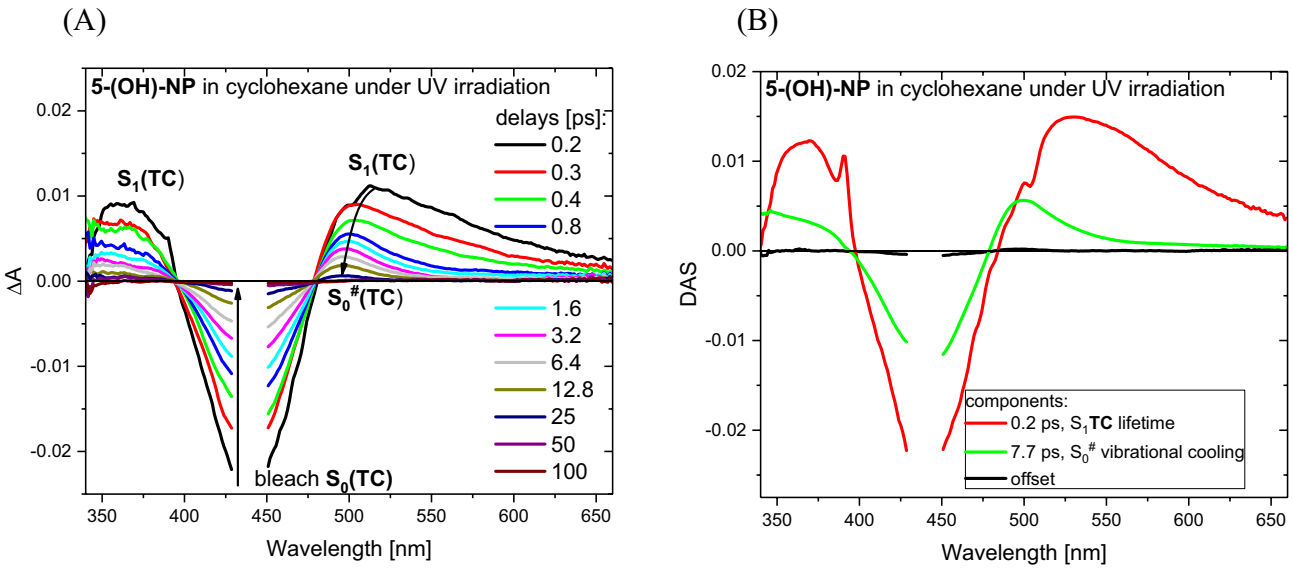

Figure 5. (**A**) UV–Vis transient absorption spectra recorded for **TC** solution in cyclohexane upon the laser pulse excitation at λ = 444 nm. PSS with a constant **TC** population was achieved by a continuous irradiation of **5-(OH)-NP** cyclohexane solution with LED at λ = 340 nm. (**B**) Decay associated spectra obtained with global analysis using bi-exponential function.

S_1-state minimum (see Table S1) is one of the smallest θ_1 values for derivatives we have studied[40,41], which makes the **5-(OH)-NP** molecule well situated for suppression of **TT** formation.

Confirmation of ESIPT by ultrafast transient absorption studies. To confirm the ESIPT process predicted by theory in the gas phase, for experimental work the inert solvent cyclohexane was selected. Thus, for ultrafast studies, a solution of **5-(OH)-NP** in cyclohexane was prepared and the sample was continuously irradiated by LED at 340 nm to generate a photostationary state (PSS). As described above, in PSS practically the only colored form is **TC**. In the pump-probe experiment, a laser-pulse excitation wavelength of 444 nm was chosen for selective **TC** photoexcitation. Figure 5A shows UV–Vis transient absorption recorded in the time window from 0.2 to 100 ps.

At the initial delay of 0.2 ps the positive bands at 360 and 520 nm are clearly observed. Two assignments for these bands can be considered. One is that the initial positive spectrum belongs to the population product—**TC*-proton transferred**, since the transfer of the proton can be faster than our temporal resolution (< 200 fs), in agreement with theoretical calculations (barrierless process) and the ultrafast character of such processes in analogous molecular systems (3-hydroxyflavone[27]). But such an assignment does not agree with the calculated electronic transition $S_1 \rightarrow S_n$ for **TC*-proton transferred** (see Table S2). The alternative assignment for the initial positive band is **TC***. Indeed, the spectral shape is reminiscent of the recorded data for **TC*** from **5-(H)-NP**[54]. Thus, the positive bands at 360 and 520 nm correspond to $S_1 \rightarrow S_n$ and $S_1 \rightarrow S_m$ transitions of **TC*** population (n > m), while the negative band peaking at about 440 nm can be attributed to **TC** bleaching. On the basis of global analysis (Fig. 5B), the **TC** excited-state lifetime is only 0.2 ps vs. 0.8 ps (**5-(OH)-NP** vs. **5-(H)-NP**). This shortened **TC** lifetime effect can be explained by ESIPT, which drives the system toward the conical intersection $CI(S_1/S_0)$ region much faster. The proton-transferred **TC** excited state is not observed in the experiment due to a low instantaneous concentration. The back proton transfer occurring in the S_0 state is barrierless according to calculations, so that it also probably has ultrafast character[56]. Thus, the evolution of transient spectra 0.8–100 ps (Fig. 5A) reflects vibrational cooling of the nascent hot **TC** species in the electronic ground state $S_0^{\#}$. The spectrally wide $S_0^{\#}$ **TC** absorption band in comparison to the vibrationally relaxed S_0 **TC** absorption band is an expected feature[57]. The time-constant of vibrational cooling is 7.7 ps obtained from global fitting (Fig. 5B).

TC excited state deactivation in polar and hydrogen-bonding solvents. Upon changing from cyclohexane to methanol solution, the recorded transient absorption spectra are similar (Fig. S6), but the population of **TC** in the singlet excited state shows a longer lifetime (0.8 ps in methanol *vs.* 0.2 ps in cyclohexane, Table S3), suggesting ESIPT in that solvent, if present, is a minor deactivation path. Moreover, one would expect a slower ESIPT for **5-(OD)-NP** in MeOD than for **5-(OH)-NP** in MeOH, due to the difference in mass between deuterium and hydrogen, as reported in other molecular systems[58,59]. However nearly identical transient absorption spectra and kinetics were collected for **5-(OD)-NP** (in MeOD) and **5-(OH)-NP** (in MeOH), which supports the hypothesis of minor ESIPT involvement in these solvents due to a high competition from internal conversion $S_1 \rightarrow S_0$ caused by a change in the **TC** S_1 geometry in the $C_{14}{=}C_1{-}C_2{=}C_3$ bridge, by analogy with **5-(H)-NP**[39,54]. In the polar acetonitrile, the transient absorption spectra for **TC** are similar to those in cyclohexane and methanol. The **TC** S_1 state lifetime is 0.5 ps in acetonitrile (Fig. S7), thus longer than in cyclohexane (0.2 ps), but shorter in

relation to methanol (0.8 ps, Table S3). To rationalize the decrease of τ_{S1} in acetonitrile *vs.* methanol, we note that the **TC** S_1 state dipole moment is substantially high (Table 1). Thus, one expects that the high acetonitrile polarity exerts a stabilizing effect for **TC** in the excited state and $S_1 \rightarrow S_0$ internal conversion is facilitated. In methanol, on the other hand, strong solute–solvent specific interactions can slow down the geometry evolution needed for reaching the conical intersection, responsible for $S_1 \rightarrow S_0$ internal conversion. Interestingly, in acetonitrile and methanol τ_{S1} **TC*** lifetimes are longer for **5-(OH)-NP** than **5-(H)-NP** (Table S3). The presence of the hydroxy group strengthens solute–solvent interactions, thereby hampering the change in **TC*** geometry.

Conclusions

Calculations in the gas phase show that the ESIPT process predominates in **TC** S_1 state deactivation over the **TC** → **TT** photoisomerization, hindering formation of the **TT** isomer. Internal conversion ($S_1 \rightarrow S_0$) may take place during the ESIPT process before the double-bond rotations are activated in the excited state. The ESIPT process is experimentally observed in cyclohexane by a shortening of the singlet excited **TC** lifetime to 0.2 ps in relation the unsubstituted compound (0.8 ps for **5-(H)-NP**[54]). Such fast dynamics of ESIPT has been reported in structurally related 3-hydroxychromone[26]. In other solvents, such as methanol or acetonitrile, ESIPT plays a less important role in **TC** excited state deactivation, since the intramolecular hydrogen bond is disrupted by solute–solvent specific interaction. The polar **TC** S_1 species is stabilized by solvent polarity, and the **TC** S_1 deactivation mainly occurs through the internal conversion process $S_1 \rightarrow S_0$ induced by a change in geometry upon activation of the two double bonds present in the C_{14}=C_1–C_2=C_3 bridge. Stabilization of **TC** S_1 species in polar solvent lowers the S_1-state potential-energy profile (vs. S_0-state), thus the conical intersection CI(S_1/S_0) produces the S_0 state with less advanced change in the C_{14}=C_1 twist angle. Consequently, **TT** formation is disfavoured. On the other hand, different types of solvent-molecule interactions (dipole–dipole, π–π stacking and hydrogen bonding) slow down the **TC*** geometry evolution towards the conical intersection CI (S_1/S_0).

These main pathways (ESIPT or polarity-mediated IC) appear to reduce photoisomerization via the channel **TC** → **TT**. This explains the reduction of the **TT** population in the photochromic reaction using continuous UV irradiation performed for **5-(OH)-NP** in comparison to the parent compound **5-(H)-NP**.

An unintended consequence of 5-hydroxy substitution is a weak residual color in **5-(OH)-NP** solutions due to the presence of small quantities (ca. 1%) of the colored **TC** isomer produced through thermal equilibrium in cyclohexane solution. This is a result of the intramolecular hydrogen bond present in the structure, stabilizing its relative energy *vs*. the closed colorless form **CF**. Breaking the intramolecular hydrogen bond in methanol or acetonitrile by solute–solvent specific interactions shifts the equilibrium towards **CF**.

Data availability

The datasets generated during the current study are available from the corresponding author on request.

Received: 18 August 2022; Accepted: 4 November 2022
Published online: 10 November 2022

References

1. Chou, P.-T. & Solntsev, K. M. Photoinduced proton transfer in chemistry and biology. *J. Phys. Chem B* **119**, 2089. https://doi.org/10.1021/jp510024r (2015).
2. Esboui, M., Jaidane, N. & Lakhdar, B. Excited state proton transfer in 2-hydroxypyridine–ammonia clusters: Theoretical investigation. *Chem. Phys. Lett.* **430**, 195–203. https://doi.org/10.1016/j.cplett.2006.08.119 (2006).
3. Ataelahi, M., Omidyan, R. & Azimi, G. Photophysics and photochemistry of *cis*- and *trans*-hydroquinone, catechol and their ammonia clusters: A theoretical study. *Photochem. Photobiol. Sci.* **14**, 457–464. https://doi.org/10.1039/c4pp00356j (2014).
4. Sobolewski, A. L. & Domcke, W. *Ab initio* studies on the photophysics of the guanine–cytosine base pair. *Phys. Chem. Chem. Phys.* **6**, 2763–2771. https://doi.org/10.1039/b314419d (2004).
5. Perun, S., Sobolewski, A. L. & Domcke, W. Role of electron-driven proton-transfer processes in the excited-state deactivation of the adenine-thymine base pair. *J. Phys. Chem A* **110**, 9031–9038. https://doi.org/10.1021/jp061945r (2006).
6. Zhang, Y., de La Harpe, K., Beckstead, A. A., Improta, R. & Kohler, B. UV-Induced proton transfer between DNA strands. *J. Am. Chem. Soc.* **137**, 7059. https://doi.org/10.1021/jacs.5b03914 (2018).
7. Wilbraham, L., Savarese, M., Rega, N., Adamo, C. & Ciofini, I. Describing excited state intramolecular proton transfer in dual emissive systems: A density functional theory based analysis. *J. Phys. Chem. B* **119**, 2459. https://doi.org/10.1021/jp507425x (2015).
8. Houari, Y. *et al.* Modeling optical signatures and excited-state reactivities of substituted hydroxyphenylbenzoxazoles (HBO) ESIPT dyes. *Phys. Chem. Chem. Phys.* **16**, 1319–1321. https://doi.org/10.1039/C3CP54703E (2014).
9. Luber, S., Adamczyk, K., Nibbering, E. T. J. & Batista, V. S. Photoinduced proton coupled electron transfer in 2-(2'-hydroxyphenyl)-benzothiazole. *J. Phys. Chem. A* **117**, 5269–5279. https://doi.org/10.1021/jp403342w (2013).
10. Stasyuk, A., Banasiewicz, M., Cyranski, M. K. & Gryko, D. T. Imidazo[1,2-a]pyridines susceptible to excited state intramolecular proton transfer: One-pot synthesis via an Ortoleva-King reaction. *J. Org. Chem.* **77**, 5552. https://doi.org/10.1021/jo300643w (2012).
11. Karsili, T. N. V., Marchetti, B., Ashfold, M. N. R. & Domcke, W. *Ab initio* study of potential ultrafast internal conversion routes in oxybenzone, caffeic acid, and ferulic acid: implications for sunscreens. *J. Phys. Chem. A* **118**, 11999–12010. https://doi.org/10.1021/jp507282d (2014).
12. Sobolewski, A. L., Domcke, W. & Hattig, C. Photophysics of organic photostabilizers. *Ab initio* study of the excited-state deactivation mechanisms of 2-(2'-hydroxyphenyl)benzotriazole. *J. Phys. Chem A* **110**, 6301–6306. https://doi.org/10.1021/jp0574798 (2006).
13. Otterstedt, J. A. Photostability and molecular structure. *J. Chem. Phys.* **58**, 5716. https://doi.org/10.1063/1.1679196 (1973).
14. Heller, H. J. & Blattmann, H. R. Some aspects of the light protection of polymers. *Pure Appl. Chem.* **30**, 145. https://doi.org/10.1351/pac197230010145 (1972).
15. Heller, H. J. & Blattmann, H. R. Some aspects of stabilization of polymers against light. *Pure Appl. Chem.* **36**, 141. https://doi.org/10.1351/pac197336010141 (1973).
16. Ziolek, M., Burdzinski, G., Filipczak, K., Karolczak, J. & Maciejewski, A. Spectroscopic and photophysical studies of the hydroquinone family of photochromic Schiff bases analyzed over a 17-orders-of-magnitude time scale. *Phys. Chem. Chem. Phys.* **10**, 1304–1318. https://doi.org/10.1039/b715244b (2008).

17. Sobolewski, A. L. Reversible molecular switch driven by excited-state hydrogen transfer. *Phys. Chem. Chem. Phys.* **10**, 1243–1247. https://doi.org/10.1039/b716075e (2008).
18. Rode, M. F. & Sobolewski, A. L. Effect of chemical substituents on energetical landscape of a molecular switch: an *ab initio* study. *J. Phys. Chem. A* **114**, 11879–11889. https://doi.org/10.1021/jp105710n (2010).
19. Rode, M. F. & Sobolewski, A. L. *Ab initio* study on the excited state proton transfer mediated photophysics of 3-hydroxy-picolinic acid. *Chem. Phys.* **409**, 41–48. https://doi.org/10.1016/j.chemphys.2012.10.001 (2012).
20. Georgiev, A. *et al.* 7-OH quinoline Schiff bases: Are they the long awaited tautomeric bistable switches?. *Dyes Pigm.* **195**, 109739. https://doi.org/10.1016/j.dyepig.2021.109739 (2021).
21. Nakashima, K. *et al.* Solvent-triggered long-range proton transport in 7-hydroxyquinoline using a sulfonamide transporter group. *J. Org. Chem.* **87**, 6794–6806. https://doi.org/10.1021/acs.joc.2c00494 (2022).
22. Csehi, A., Halasz, G. J. & Vibok, A. Molecular switch properties of 7-hydroxyquinoline compounds. *Int. J. Quant. Chem.* **114**, 1135–1145. https://doi.org/10.1002/qua.24639 (2014).
23. Berenbeim, J. A. *et al.* Excited state intramolecular proton transfer in hydroxyanthraquinones: Toward predicting fading of organic red colorants in art. *Sci. Adv.* **5**, eaaw227. https://doi.org/10.1126/sciadv.aaw5227 (2019).
24. Sobolewski, A. L. & Domcke, W. Photophysics of eumelanin: Ab initio studies on the electronic spectroscopy and photochemistry of 5,6-dihydroxyindole. *ChemPhysChem* **8**, 756–762. https://doi.org/10.1002/cphc.200600768 (2007).
25. Nag, P. & Vennapusa, S. R. Substitution-independent proton transfer in hydroxychromones. *J. Photochem. Photobiol.* **431**, 114024. https://doi.org/10.1016/j.jphotochem.2022.114024 (2022).
26. Chevalier, K. *et al.* ESIPT and photodissociation of 3-hydroxychromone in solution: Photoinduced processes studied by static and time-resolved UV/Vis, fluorescence, and IR spectroscopy. *J. Phys. Chem. A* **117**, 11233–11245. https://doi.org/10.1021/jp407252y (2013).
27. Ameer-Beg, S. *et al.* Ultrafast measurements of excited state intramolecular proton transfer (ESIPT) in room temperature solutions of 3-hydroxyflavone and derivatives. *J. Phys. Chem. A* **105**, 3709–3718. https://doi.org/10.1021/jp0031101 (2001).
28. Yushchenko, D. A. *et al.* 2-Aryl-3-hydroxyquinolones, a new class of dyes with solvent dependent dual emission due to excited state intramolecular proton transfer. *New J. Chem.* **30**, 774–781. https://doi.org/10.1039/b601400c (2006).
29. Rode, M. F. & Sobolewski, A. L. Effect of chemical substitutions on photo-switching properties of 3-hydroxy-picolinic acid studied by ab initio methods. *J. Chem. Phys.* **140**, 084301. https://doi.org/10.1063/1.4865815 (2014).
30. Man, Z. *et al.* Excitation-wavelength-dependent organic long-persistent luminescence originating from excited-state long-range proton transfer. *J. Am. Chem. Soc.* https://doi.org/10.1021/jacs.1022c01248 (2022).
31. Barboza, C. A., Gawrys, P., Banasiewicz, M., Kozankiewicz, B. & Sobolewski, A. L. Substituent effects on the photophysical properties of tris(salicylideneanilines). *Phys. Chem. Chem. Phys.* **23**, 1156–1164. https://doi.org/10.1039/D0CP04385K (2021).
32. Kumpulainen, T., Lang, B., Rosspeintner, A. & Vauthey, E. Ultrafast elementary photochemical processes of organic molecules in liquid solution. *Chem. Rev.* **117**, 10826–10939. https://doi.org/10.1021/acs.chemrev.6b00491 (2017).
33. Uzhinov, B. M. & Khimich, M. N. Conformational effects in excited state intramlecular proton transfer of organic compounds. *Russ. Chem. Rev.* **80**, 553–577. https://doi.org/10.1070/RC2011v080n06ABEH004144 (2011).
34. Ignasiak, M. T., Houee-Levin, C., Kciuk, G., Marciniak, B. & Pedzinski, T. A reevaluation of the photolytic properties of 2-hydroxybenzophenone-based UV sunscreens: Are chemical sunscreens inoffensive?. *ChemPhysChem* **16**, 628–633. https://doi.org/10.1002/cphc.201402703 (2015).
35. Crano, J. C., Flood, T., Knowles, D., Kumar, A. & Van Gemert, B. Photochromic compounds: Chemistry and application in ophthalmic lenses. *Pure Appl. Chem.* **68**, 1395–1398. https://doi.org/10.1351/pac199668071395 (1996).
36. Hepworth, J. D. & Heron, B. M. in *Functional Dyes* (ed S.H. Kim) Ch. 3, 85–135 (Elsevier, 2006).
37. Corns, S. N., Partington, S. M. & Towns, A. D. Industrial organic photochromic dyes. *Color. Technol.* **125**, 249–261. https://doi.org/10.1111/j.1478-4408.2009.00204.x (2009).
38. Towns, A. in *Applied Photochemistry: When Light Meets Molecules* (eds G. Bergamini & S. Silvi) 227–279 (Springer International Publishing, 2016).
39. Brazevic, S., Nizinski, S., Szabla, R., Rode, M. F. & Burdzinski, G. Photochromic reaction in 3*H*-naphthopyrans studied by vibrational spectroscopy and quantum chemical calculations. *Phys. Chem. Chem. Phys.* **21**, 11861–11870. https://doi.org/10.1039/C9CP01451A (2019).
40. Brazevic, S. *et al.* Control of the photo-isomerization mechanism in 3H-naphthopyrans to prevent formation of unwanted long-lived photoproducts. *Int. J. Mol. Sci.* **21**, 7825. https://doi.org/10.3390/ijms21217825 (2020).
41. Gierczyk, B., Rode, M. F. & Burdzinski, G. Mechanistic insights into photochromic 3*H*-naphthopyran showing strong photocoloration. *Sci. Rep.* **12**, 10781. https://doi.org/10.1038/s41598-022-14679-9 (2022).
42. Inagaki, Y., Kobayashi, Y., Mutoh, K. & Abe, J. A simple and versatile strategy for rapid color fading and intense coloration of photochromic naphthopyran families. *J. Am. Chem. Soc.* **139**, 13429–13441. https://doi.org/10.1021/jacs.7b06293 (2017).
43. Wendel, M. *et al.* Time-resolved spectroscopy of the singlet excited state of betanin in aqueous and alcoholic solutions. *Phys. Chem. Chem. Phys.* **17**, 18152–18158. https://doi.org/10.1039/C5CP00684H (2015).
44. Møller, C. & Plesset, M. S. Note on an aproximation treatment for many-electron systems. *Phys. Rev* **46**, 618–622. https://doi.org/10.1103/PhysRev.46.618 (1934).
45. Hättig, C. in *Advances in Quantum Chemistry* Vol. 50 (ed H. J. Å Jensen) 37–60 (Academic Press, 2005).
46. Schirmer, J. Beyond the random-phase approximation: A new approximation scheme for the polarization propagator. *Phys. Rev. A* **26**, 2395–2416. https://doi.org/10.1103/PhysRevA.26.2395 (1982).
47. Trofimov, A. B. & Schirmer, J. An efficient polarization propagator approach to valence electron excitation spectra. *J. Phys. B At. Mol. Opt. Phys.* **28**, 2299–2324. https://doi.org/10.1088/0953-4075/28/12/003 (1995).
48. Dunning, T. H. Jr. Gaussian basis sets for use in correlated molecular calculations. I. The atoms boron through neon and hydrogen. *J. Chem. Phys.* **90**, 1007–1023. https://doi.org/10.1063/1.456153 (1989).
49. Christiansen, O., Koch, H. & Jørgensen, P. The second-order approximate coupled cluster singles and doubles model CC2. *Chem. Phys. Lett.* **243**, 409–418. https://doi.org/10.1016/0009-2614(95)00841-Q (1995).
50. Hättig, C. & Weigend, F. CC2 excitation energy calculations on large molecules using the resolution of the identity approximation. *J. Chem. Phys.* **113**, 5154–5161. https://doi.org/10.1063/1.1290013 (2000).
51. TURBOMOLE V7.1 2016, a development of University of Karlsruhe and Forschungszentrum Karlsruhe GmbH, 1989–2007, TURBOMOLE GmbH, since 2007. http://www.turbomole.com. Accessed 17 August 2022.
52. de Azevedo, O. D. C. C. *et al.* Synthesis and photochromism of novel pyridyl-substituted naphthopyrans. *J. Org. Chem.* **85**, 10772–10796. https://doi.org/10.1021/acs.joc.0c01296 (2020).
53. Brazevic, S. *et al. Cisoid-cis* intermediate plays a crucial role in decolouration rate in photochromic reaction of 8*H*-pyranoquinazolines and 3*H*-naphthopyrans. *Dyes Pigm.* **201**, 110249. https://doi.org/10.1016/j.dyepig.2022.110249 (2022).
54. Brazevic, S., Baranowski, M., Sikorski, M., Rode, M. F. & Burdziński, G. Ultrafast dynamics of the transoid-*cis* isomer formed in photochromic reaction from 3*H*-naphthopyran. *ChemPhysChem* **21**, 1402–1407. https://doi.org/10.1002/cphc.202000294 (2020).
55. Chevalier, K. *et al.* Transient IR spectroscopy and *ab initio* calculations on ESIPT in 3-hydroxyflavone solvated in acetonitrile. *Phys. Chem. Chem. Phys.* **14**, 15007–15020. https://doi.org/10.1039/c2cp41077j (2012).
56. Bader, A. N., Ariese, F. N. & Gooijer, C. Proton transfer in 3-hydroxyflavone studied by high-resolution 10 K laser-excited Shpol'skii spectroscopy. *J. Phys. Chem. A* **106**, 2844–2849 (2002).

57. Rosspeintner, A., Lang, B. & Vauthey, E. Ultrafast photochemistry in liquids. *Annu. Rev. Phys. Chem.* **64**, 247–271. https://doi.org/10.1146/annurev-physchem-040412-110146 (2013).
58. Flom, S. R. & Barbara, P. F. Proton transfer and hydrogen bonding in the internal conversion of S_1 anthraquinones. *J. Phys. Chem.* **89**, 4489–4494. https://doi.org/10.1021/j100267a017 (1985).
59. Han, G. R. *et al.* Shedding new light on an old molecule: Quinophthalone displays uncommon N-to-O excited state intramolecular proton transfer (ESIPT) between photobases. *Sci. Rep.* **7**, 3863. https://doi.org/10.1038/s41598-017-04114-9 (2017).

Acknowledgements

This work was performed with financial support from the National Science Centre (NCN), Poland, project 2017/27/B/ST4/00320, and the Polish-U.S. Fulbright Commission (Grant no. US/2021/31/SC). Calculations were performed at the PL-Grid Infrastructure.

Author contributions

The following co-authors contributed in particular with; B.G. synthesis, writing—review and editing, S.M., conceptualization, writing—review and editing, M.R. theoretical calculations, conceptualization, writing—review and editing and G.B. spectroscopic experiments, formal analysis, supervision, funding acquisition, conceptualization, writing—review and editing.

Competing interests

The authors declare no competing interests.

Additional information

Supplementary Information The online version contains supplementary material available at https://doi.org/10.1038/s41598-022-23759-9.

Correspondence and requests for materials should be addressed to M.F.R. or G.B.

Reprints and permissions information is available at www.nature.com/reprints.

Publisher's note Springer Nature remains neutral with regard to jurisdictional claims in published maps and institutional affiliations.